Fractal dimension and avalanches of invasion percolation: the effect of aspect ratio

M. Ferer[a,b,*], Grant S. Bromhal[c], Duane H. Smith[c,b]

[a] *National Energy Technology Laboratory, Morgantown, WV 26507-0880, USA*
[b] *Department of Physics, West Virginia University, P.O. Box 6315, Morgantown, WV 26506-6315, USA*
[c] *US DOE, National Energy Technology Laboratory, Morgantown, WV 26507-0880, USA*

Abstract

Troubled by unreliable estimates of the fractal dimension from straightforward box-counting applied to invasion percolation in million site short-wide systems (i.e., the length in the average flow direction is the smaller dimension), we undertook a study of the effect of aspect ratio on fractal dimension determinations and on avalanche structure. In box-counting, we found evidence of a competition between the different singular behaviors associated with the bulk and the external hull (interface), which was most noticeable for the short-wide systems with a long external hull. Modifying the box-counting to exclude those boxes covering the external hull provides results for the short-wide systems which are consistent with results from the literature and from straightforward box-counting on long-narrow systems. Not surprisingly, we found that the avalanche size distribution was 'cut off' by the length in the short-wide systems; however, we also found that the distribution was cut off by the width in the long-narrow systems. Therefore, the smaller dimension served as a cut-off length for the distribution of avalanche sizes, so that in the long-narrow systems, the distribution of avalanche sizes collapses long before the injected fluid reaches the outlet. This results in fingering patterns in the long-narrow systems that are different from those in the short-wide systems where the avalanche size distribution is maintained all the way to the outlet. Determining the fractal dimension from the power-law dependence of mass upon a typical length scale was found to be unaffected by the length of the external hull, providing the standard literature values of fractal dimension for the problematic short-wide systems.

Keywords: Invasion percolation; Avalanches; Fractal dimension

* Corresponding author. Department of Physics, West Virginia University, P.O. Box 6315, Morgantown, WV 26506-6315, USA. Fax: +1-204-285-4070.
E-mail address: mferer@wvu.edu (M. Ferer).

1. Introduction

The fingering of the injected fluid associated with immiscible, two-phase flow in porous media is one of the major reasons for the inefficiency of several important geologic recovery/remediation processes. In secondary oil recovery, water displaces much less than half of the oil in any given formation, because the water 'fingers' into the oil-saturated reservoir. In CO_2 sequestration (a means to mitigate global warming), where carbon dioxide is injected into brine-saturated porous media (e.g. sub-sea floor formations, deep saline aquifers) for long-term storage, fingering limits the available storage capacity so that only a small fraction of the reservoir is occupied by CO_2. In remediation of DNAPL spills, which can enter and contaminate the groundwater, standard pump and treat remediation methods are often ineffective because water flushing in porous media typically mobilizes only a small portion of the pollutant; a better understanding of the location of the DNAPL within the water table can improve this process. Our focus in all of these processes is on the efficiency of displacement, so it is important to understand how the injected fluid occupies the medium. Therefore, this study focuses on the saturation of a non-wetting fluid injected into porous media—its fingering, and its fractal character.

For decades, it has been accepted that displacement efficiency can depend strongly upon injection rates, i.e., capillary numbers, $N_c = (\text{viscous forces})/(\text{capillary forces})$, where the capillary forces dominate over viscous forces [1]. In practical injection situations, low velocities are found far from the injection well-bore where the fluid spreads radially and gradually slows down. In the extreme limit of infinitesimal injection rate, effectively $N_c = 0$, Wilkinson and others introduced a simple model of immiscible, two-phase flow called invasion percolation (IP) [2,3]. In this model, the non-wetting, injected fluid advances solely through the largest throat (the one with the smallest capillary pressure) on the interface between the injected, non-wetting fluid and the wetting, defending fluid during each time step. Far from the injection well, where the simple model should be most applicable, the interface is becoming longer and longer so that there are more and more interfacial throats through which flow may occur.

Far from the injection well, as velocities approach zero, viscous effects may be neglected, so that the pressures are uniform throughout any one fluid. One can imagine drawing a box around such an interface location and studying the properties of the fluids at those locations as they move. The pressure in the injected fluid is uniformly equal to the pressure at the inlet of such a box, while the pressure in the wetting fluid is uniformly equal to the outlet pressure. The pressure drop at the interface (inlet pressure minus outlet pressure) is adjusted to be just large enough to advance the non-wetting fluid through the largest allowed throat on the interface. Therefore, this pressure drop must always be positive and the wetting fluid cannot displace the non-wetting fluid from an occupied pore-body. Since the wetting fluid cannot displace the non-wetting fluid, a fully encircled region of wetting fluid is immobilized or trapped, in that the non-wetting fluid is prevented from advancing into this trapped region. Invasion percolation with trapping (IPwt) modifies the standard IP rules to forbid advance into a 'trapped' region [4–7]. A number of these 'trapped' regions can be seen near the inlet of the pattern in Fig. 1. Recently, we have presented results from a standard pore-leve model of

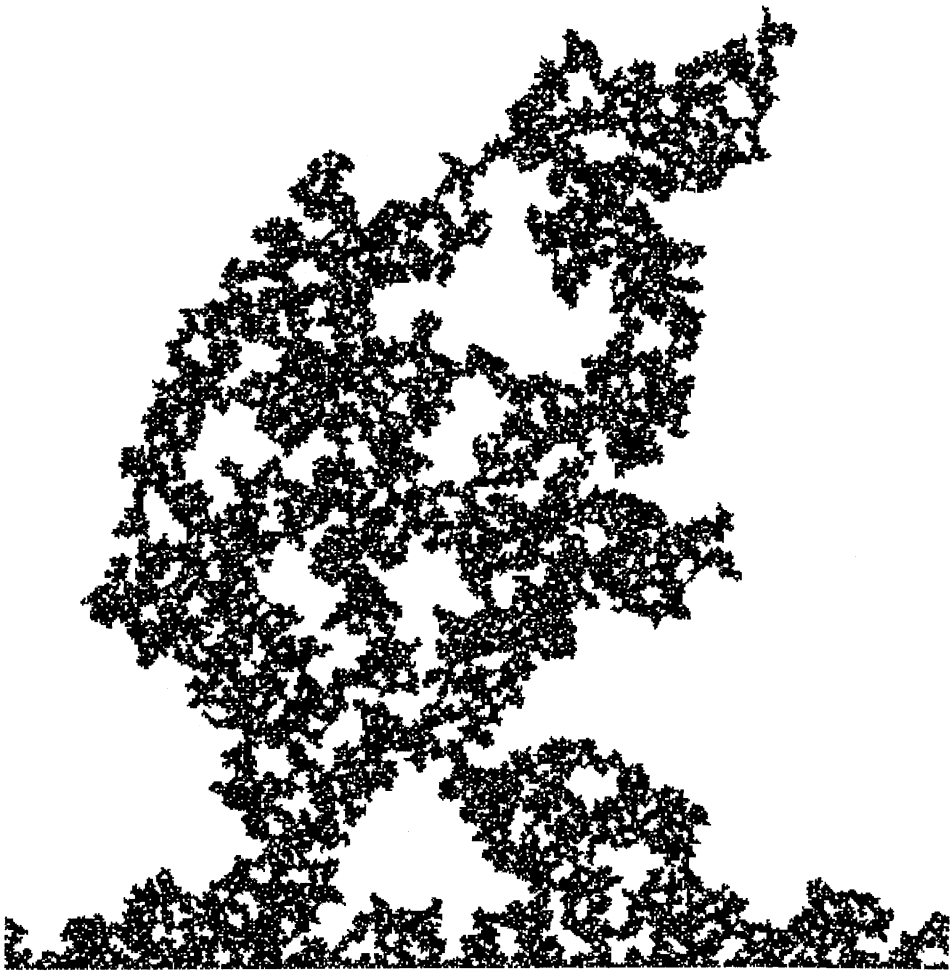

Fig. 1. A characteristic IPwt pattern occupying more than 2×10^5 lattice sites in a porous medium with more than a million lattice sites (size 1440×720).

two-phase flow in porous media, which shows that the model reproduces saturations and flow patterns from IPwt in the limit of small capillary number [8].

This IPwt model has been widely studied since its introduction [2,3,7,9–13]. There have also been many applications of this model and closely related models to a variety of increasingly more complex porous media flow problems [14–16]; Blunt [17] has provided an excellent review of the most recent work. The injection patterns have been shown to be self-similar fractals with a value of fractal dimension close to that of the standard percolation model. Recent work on larger systems favors a value of fractal dimension below that of ordinary critical percolation theory, $D_f \approx 1.82$, with uncertainties that do not overlap the ordinary critical percolation theory value, $D_f \approx 1.89$

[5,7,13,18]. Other studies, typically on smaller systems, indicate that $D_f \approx 1.89$ is a better fit to the observed results [19–21]. A recent paper performed simulations on lattices with more that 250 million sites and used a correction to scaling to account for any remaining size dependence. This paper argues convincingly that the fractal dimension of IPwt should be 1.825 ± 0.004 [13].

The flow in the IPwt model exhibits phenomena, variously called 'bursts', 'Haines jumps', or 'avalanches', where the advance of the interface occurs in a localized region. In this region, capillary pressures are lower than anywhere else on the interface. These avalanches were first studied in sandpile models of self-organized criticality (SOC) [22,23]. The sandpile models were found to self-organize to a critical point where avalanches of all sizes occurred and where the size distribution of these avalanches obeyed a power law. These avalanches were observed in IPwt [12]; and a scaling theory was developed to describe the number distribution and the correlations of these avalanches [11]. In a recent paper, we investigated the causes of the characteristic IPwt fingering. In studying the spatial distribution of the avalanches, we found a size cut off depending upon the distance of the avalanches from the inlet. This cut-off signals that finite-size systems cannot have achieved SOC, with avalanches at all size. Furthermore, we found that the average size (mass) of these avalanches, $\langle M_a \rangle$, increased with their average distance, $\langle x \rangle$, from the inlet as $\langle M_a \rangle \approx \langle x \rangle^{1.1}$. As a result, larger avalanches will tend to occur at the end of longer fingers causing preferential growth of these long fingers at the expense of the shorter fingers, thereby explaining the characteristic IPwt fingering.

Our previous work relied upon the time dependence of the average position, $\langle x(t) \rangle$, and saturations, $S(x,t)$ of the injected fluid because of our focus on the time-dependent occupation of the reservoir. In fractal models, the fractal dimension determines these functional dependencies; for these systems with linear injection

$$\langle x(t) \rangle = At^{1+\varepsilon} , \tag{1}$$

where $1 + \varepsilon = 1/(D_f - 1)$ and

$$S(x,t) = t^{-\varepsilon} f(x/t^{1+\varepsilon}) , \tag{2}$$

where the time is proportional to the injected mass (or volume) and $f(x/t^{1+\varepsilon})$ is an unspecified function. Eq. (1) is equivalent to the familiar relation between the mass of a linear-injection fractal such as the one in Fig. 1 and its linear dimension

$$M = C\langle x \rangle^{D_f - 1} \tag{3}$$

and Eq. (2) is a consequence of this relationship. In our earlier paper [21], these relationships as well as the space–time correlations [11,12] seemed to be more consistent with a value of fractal dimension, $D_f \approx 1.89$, closer to that of ordinary percolation [5] and less consistent with the widely accepted value, $D_f \approx 1.82$, from studies on much larger systems [5,7,13,18].

We have performed IPwt simulations for a number of systems with approximately one million sites but with significantly different aspect ratios (i.e., the ratio of length to width, length/width). In Sections 2 and 4, we compare several methods of determining the fractal dimension for these simulations: box-counting in Section 2, and mass vs.

various characteristic lengths in Section 4. We find the box-counting results to be sensitive to aspect ratio, while the other methods seem less so. This sensitivity of box-counting to aspect ratio is also seen in a simple Koch curve pattern [18]. In Section 3, we study the effect of aspect ratio upon the avalanche structure. Here, we find that for flow in narrow systems the avalanche structure is cut off long before the flow reaches the outlet; by the time the flow has advanced a distance approximately equal to the width of the system, the avalanche distribution collapses. This suggests that narrow IPwt systems cannot achieve SOC, thus altering the fingering structure.

2. Box-counting determinations of fractal dimension: effect of aspect ratio

In performing straight-forward box-counting for IPwt simulations on lattices which are short (in the average flow direction) and wide (perpendicular to the flow), we found a value for the fractal dimension which is much smaller than the accepted values. Results are presented for 'short-wide' diamond lattices, which are 400 lattice spacings $\times 2500$ spacings, 360×2520, and 720×1440 [21]. [1] A portion (approximately one-fifth of the total width) of one of these patterns is shown in Fig. 2.

The box-counting value of the fractal dimension for these short-wide systems is consistently low, predicting $D_f \approx 1.75$. In these short-wide systems, there are a large number of sites on the outer hull (those sites on the interface where the displaced fluid has a continuous path to the outlet—as opposed to sites on the interface enclosing a trapped region). The flow pattern for one of the long-narrow (2520×360) simulations is shown in Fig. 3. For these long-narrow systems, with fewer sites on the outer hull,

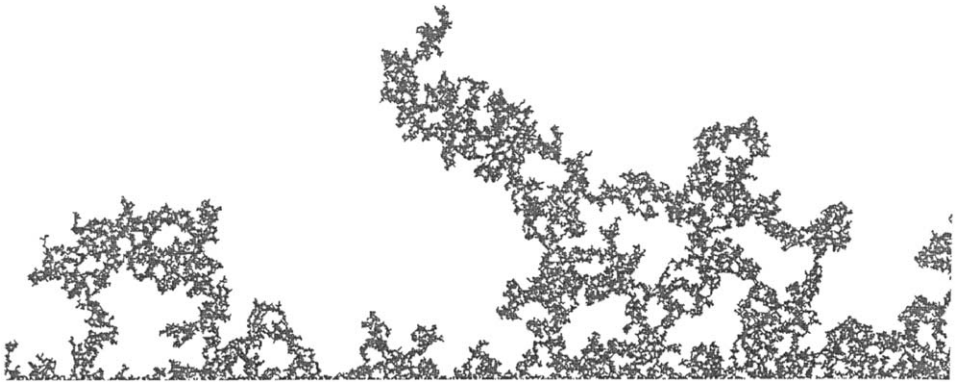

Fig. 2. A fifth of the width of a typical short-wide (400×2500) IPwt simulation. The breakthrough finger is in this fifth of the pattern.

[1] It should be noted that the 'lengths' in these system sizes are in units of the nearest-neighbor distance and are measured along a lattice diagonal (45° to the flow direction). However, the 'widths' do measure the distance perpendicular to the flow being in units of $\sqrt{2}$ times a lattice spacing.

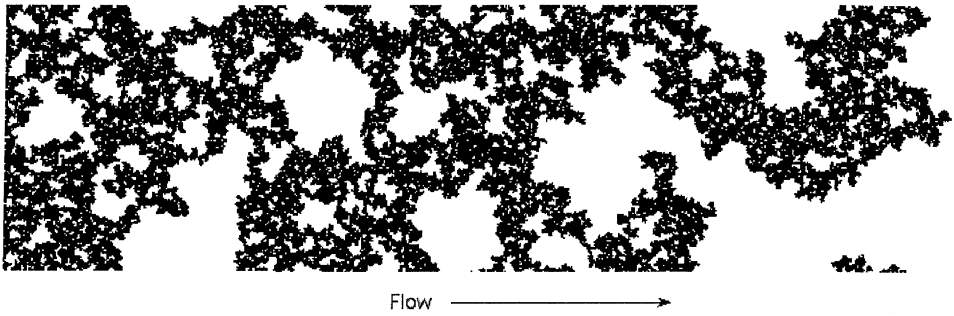

Fig. 3. The flow pattern (injection from the left—flow to the right) for a long-narrow system (2520×360). Note the periodic boundary conditions connecting the upper edge with the lower edge. Note that there are many fewer sites on the outer hull (those interfacial sites which are connected to the outlet on the right as opposed to the interfacial sites on the left hand side of the figure which are enclosing trapped regions).

box-counting produces a value of fractal dimension, $D_f \approx 1.80$, consistent with the values from some recent works [5,7,13,18].

When one does box-counting for the hull sites, one covers an $L \times L$ region with δ^2 boxes of side L/δ and counts the number of these boxes which enclose an outer-hull site. This number grows as $N_{\text{hull}}(\delta) \approx \delta^{1.75}$ [24–27]. When one does box-counting for the bulk, one counts the number of boxes which enclose any part of the injected fluid pattern; ideally, this should grow as $N_{\text{bulk}}(\delta) \approx \delta^{D_f}$. It seems likely that there may be a competition between these two power laws, because the outer hull boxes are a subset of bulk boxes. Because of this conjectured competition, one might expect that the box-counting for the bulk would predict a lower, effective value for the fractal dimension for the short-wide systems with a larger outer hull. To investigate this conjecture, we present results of box-counting for IPwt simulations with a variety of aspect ratios. But, first we present results from the box-counting for the case of a Euclidean bulk behind a fractal Koch curve [7]. The results of box-counting is presented in figures showing both $\ln(N)$ vs. $\ln(\delta)$ as well as $\ln(N_{\text{bulk}} - N_{\text{hull}})$ vs. $\ln(\delta)$, which attempts to reduce any such competition between the hull and bulk power laws.

To test this procedure on a simple fractal, we have produced the Koch curve pattern shown in Fig. 4. The curve (outer hull) has the fractal dimension $D_f = \ln(4)/\ln(3) \approx 1.26$. Of course the bulk below this fractal curve is Euclidean with dimension, $d = 2$. Thus, the number of hull sites grows as $N_{\text{hull}}(\delta) \approx \delta^{1.26}$, and box-counting for the bulk should ideally predict a Euclidean dimension of 2. Our conjecture would predict a competition between the fractal power law of the curve and the Euclidean power law for the bulk below the curve, so that straight-forward box-counting for the bulk would lead to a value of the dimension less than 2.

Fig. 5a shows the results of box-counting for the center third where the two sets of data points nearly overlap because there are many more boxes covering the bulk than the curve (i.e., $N_b \gg N_{\text{int}}$). For this center third, there should be relatively little competition. Although the plots of $\ln(N_b)$ and $\ln(N_b - N_{\text{int}})$ are nearly identical, the slope of the mid-range values of δ predict a dimension of 1.97 from straight-forward

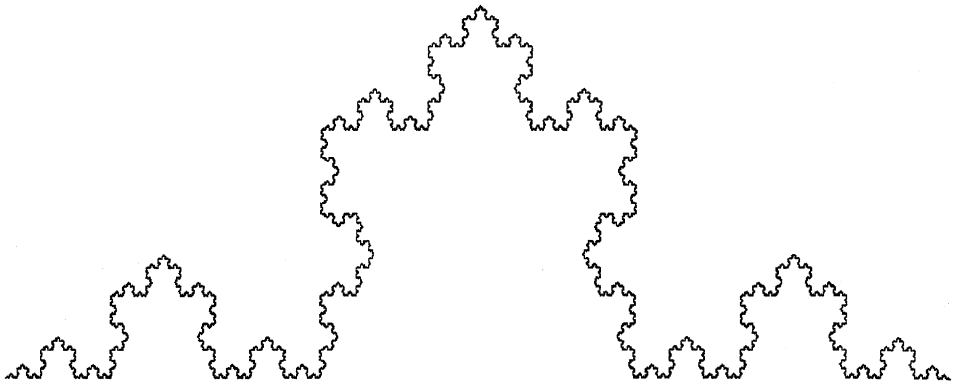

Fig. 4. A Koch curve with seven generations of the standard 3–4 Koch transformation.

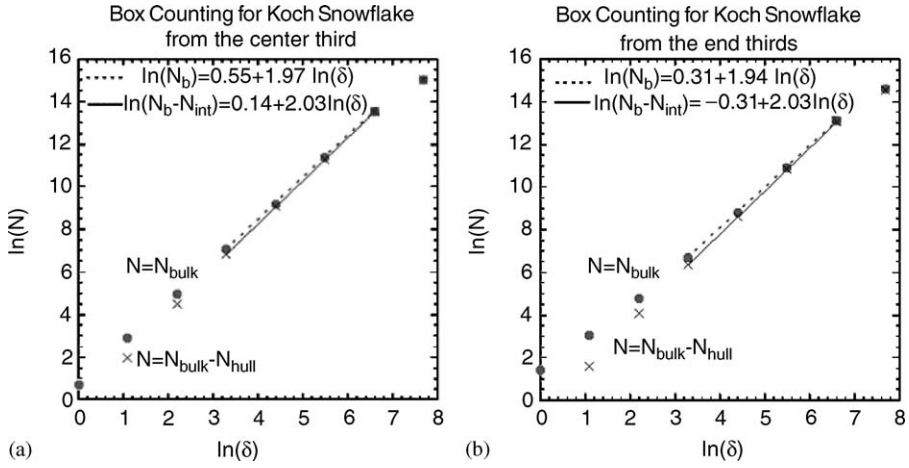

Fig. 5. The plots of $\ln(N_b)$ and $\ln(N_b - N_{int})$: (a) for the center third of the Koch pattern in Fig. 4; (b) for the two end thirds of Fig. 4; Typically, we have chosen to fit the mid-range linear regions avoiding the well-known problems associated with the small δ (large boxes) and the large δ (small boxes) extremes.

box-counting for the bulk (i.e., $\ln(N_b)$) and a value 2.03 from $\ln(N_b - N_{int})$. This suggests that using $N_b - N_{int}$ overcompensates slightly for the competition, which for this case is the same amount by which N_b underestimates the fractal dimension.

Fig. 5b shows the results of box-counting for the end third where there are many fewer boxes covering the bulk than there were in Fig. 5a. Still, there are many more boxes covering the bulk than the curve (i.e., $N_b \gg N_{int}$). For these end thirds, there should be somewhat more competition. Here, the slope of the mid-range values of δ predict a dimension of 1.94 from straight-forward box-counting for the bulk (i.e.,

$\ln(N_b)$) and a value 2.03 from $\ln(N_b - N_{int})$. Therefore, although using $N_b - N_{int}$ overcompensates slightly for the competition, its use provides a more accurate estimate of the fractal dimension than does straightforward use of N_b.

For IPwt, the case of real interest, there can be many more hull sites than there were in the case of the Koch curve. Figs. 6a–d present box-counting results for IPwt simulations with "different aspect rations". In Figs. 6a and b, straightforward box-counting for the bulk yields values of the fractal dimensions of 1.725 for the short-wide system and 1.80 for the long-narrow system. Attempting to remove possible competition due to the outer-hull boxes, the plots of $N_{bulk} - N_{hull}$ yield values of fractal dimension which are a more consistent 1.85 and 1.89.

In the cases shown in Figs. 6c and d, there is less of a difference between the aspect ratios (1:2 vs. 2:1) than in the previous case where the aspect ratios were 1:7 and 7:1. Straightforward box-counting for the bulk yields values of the fractal dimensions of 1.77 for both. Attempting to remove possible competition from the outer-hull boxes, the plots of $N_{bulk} - N_{hull}$ yield values of fractal dimension approximately 1.92.

Again in Fig. 6e, straightforward box-counting for the bulk in a short-wide system yields too small a value of the fractal dimension, 1.70, while the plot of $N_{bulk} - N_{hull}$ yields a value of 1.81 closer to the expected range $1.80 < D_f < 1.90$. A different complication in fractal dimension determination resulted from the size of the probe used [28].

It should be added that box-counting for the external perimeter of the IPwt systems discussed above led to a value of the fractal dimension of the external perimeter in agreement with the predicted $\frac{4}{3}$; we found values in the range 1.33 ± 0.04. Also, box-counting for the length of the Koch curve led to a value $D_f = 1.26 \pm 0.03$ in agreement with the exact value $\ln(4)/\ln(3) = 1.262$.

Clearly, the effect of the hull boxes is more significant for the short-wide IPwt systems, because the outer hull is so much larger in these systems. All of these results support our conjectured competition between the power laws for the number of outer-hull boxes and the number of bulk boxes, allowing more consistent estimates of the bulk fractal dimension from systems with widely differing aspect ratios. The experience with the Koch curve box-counting leads us to expect: (i) that N_{bulk} box-counting will underestimate the fractal dimension, even with relatively few hull sites, and (ii) that $N_{bulk} - N_{hull}$ box-counting will only slightly overestimate the fractal dimension. Therefore, we expect that the N_{bulk} box-counting values, $D_f \approx 1.80$, for the long-narrow systems Figs. 6b and d, may be bit low, while the $N_{bulk} - N_{hull}$ box-counting values, $D_f \approx 1.90$, for these same long-narrow systems may be a bit high. The results above seem to favor a value of fractal dimension closer to that of ordinary percolation theory, $D_f \approx 1.89$; conservatively, we estimate $D_f = 1.85 \pm 0.05$ for these small systems.

3. Aspect ratio: the effect on avalanche structure

Since the seminal work of Bak et al. [22,23], it has been appreciated that many dynamical systems achieve a self-organized critical point characterized by avalanches

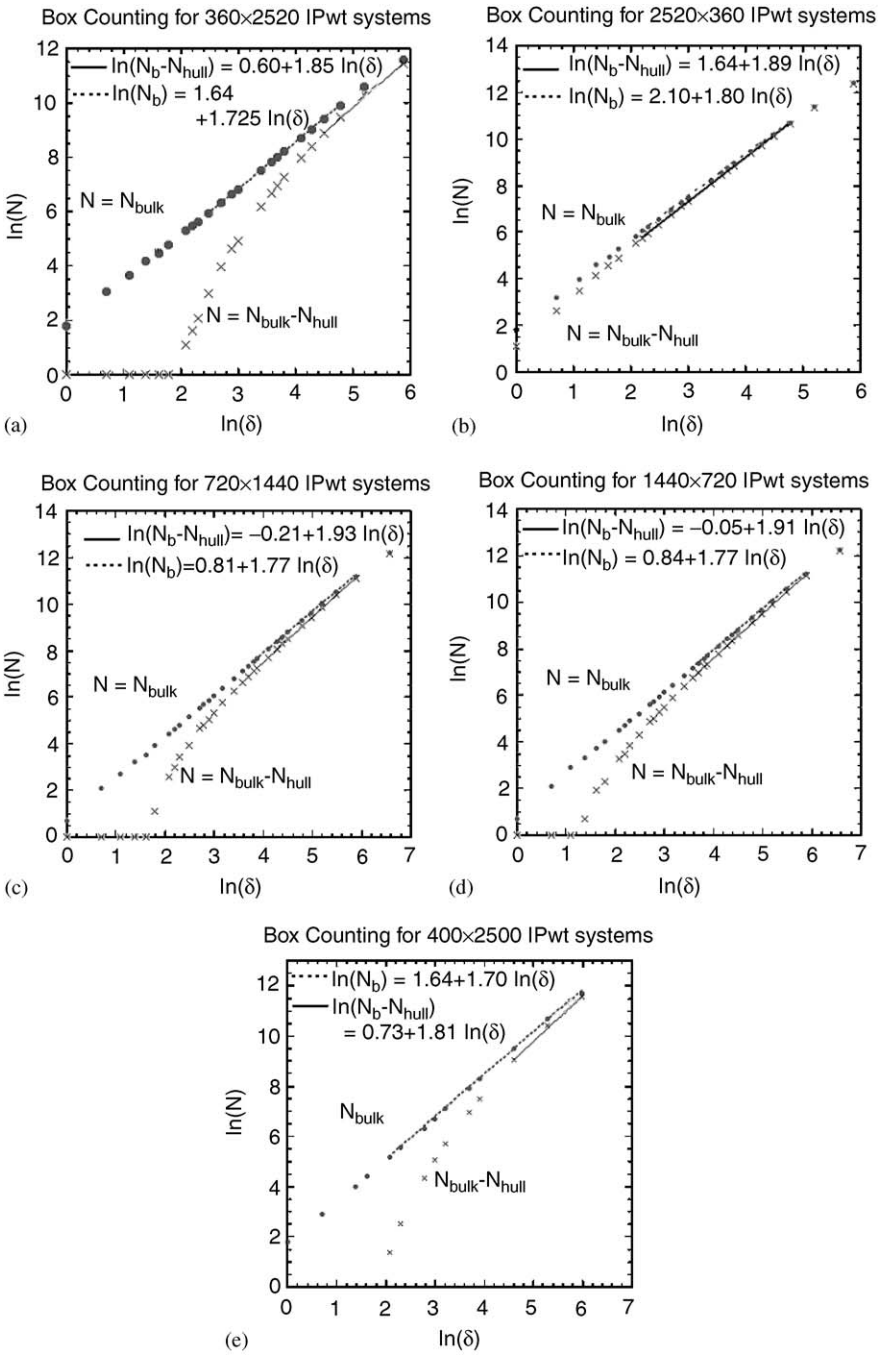

Fig. 6. ((a) and (b)) The results from box-counting for a short-wide (360×2520) system and a long-narrow (2520×360) system. ((c) and (d)) The results from box-counting for another short-wide (720×1440) and a long-narrow (1440×720). (e) The results from box-counting for another short-wide (400×2500) system.

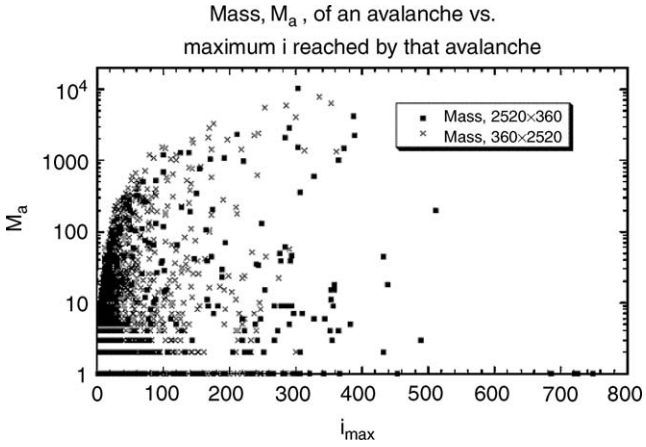

Fig. 7. The mass of all the avalanches vs. their greatest distance from the inlet, i_{max}, for a short-wide system ($360 \times 2520 \times$) and a long-narrow system (2520×360 ■).

of all sizes distributed according to a critical power law. The avalanche structure of invasion percolation was studied in two papers which found characteristic scaling of the short-time density–density correlations [11,12,21]. In a recent paper, we reproduced the results of the previous work for short-wide IPwt systems [21]. In addition, we studied the spatial distribution of avalanches, and found that avalanche size was cut off by the distance, x, from the inlet so that one could have avalanches of all sizes (necessary for criticality) only for very large systems. We also found that the average size of avalanches, $\langle M_a \rangle$, increases with their average distance $\langle x \rangle$ from the inlet, $\langle M_a \rangle \propto \langle x \rangle^{1.1}$. This latter result explains the characteristic fingering of Invasion Percolation because the longer a finger is, the more likely it is to grow through a large avalanche than a small one; this explains the preferential growth of long fingers.

In studying the spatial distribution of avalanches for different aspect ratios, we found that the width in the long-narrow systems cuts off the size of avalanches. This can be seen in Fig. 7, which shows the size of an avalanche vs. i_{max}, where i_{max} is the greatest distance from the inlet reached by that avalanche for both a short-wide (360×2520) system and the corresponding long-narrow (2520×360) system. It is interesting that one sees avalanches at a range of sizes out to maximum length of the short-wide system, $i_{max} \approx 360$. Beyond that there are very few avalanches in the long-narrow system, suggesting that the width of the long-narrow system also effectively cuts off the avalanche distribution. For the long-narrow system, there is only one avalanche beyond the last one shown in the figure ($\text{Mass}_a = 1$ at $i_{max} = 748$). That final avalanche goes to breakthrough and has a mass, $M_a = 196\,780$. This collapse of the avalanche distribution for the long-narrow systems must result when an avalanche spans the full-width (or most of the width) so that the vast majority of the interface (external hull) resides on this avalanche, preventing the occurrence of a spatially separate avalanche. Therefore,

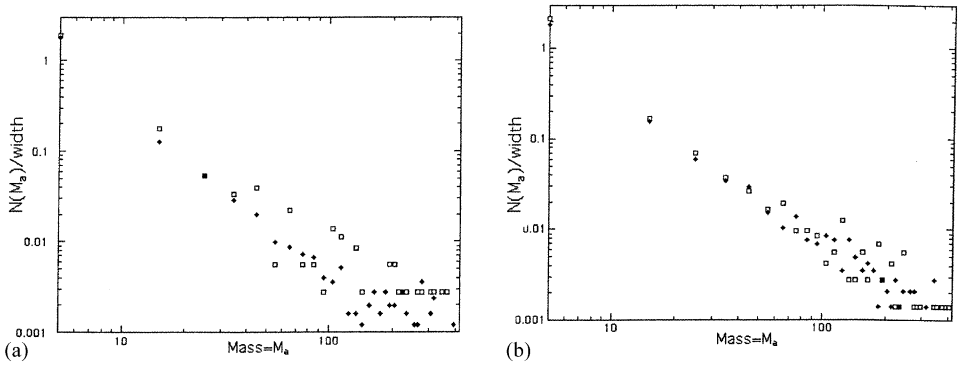

Fig. 8. The mass distribution of the avalanches for a long-narrow system (□) with whose for a short-wide system (♦) is compared. In (a) results for the 2520 × 360 and the 360 × 2520 systems and in (b) results for the 1440 × 720 and the 720 × 1440 systems are shown. We have scaled the number of avalanches of mass m by the width because the number should be proportional to the width. Also, to improve statistics, we have chosen to bin the avalanches, so that $N(5)$ is the number of avalanches with mass between 1 and 10, $N(15)$ is the number between 11 and 20, etc.

long-narrow systems cannot accurately represent the avalanche distribution of those real systems that have long interfaces.

Figs. 8a and b compare the mass distribution of the avalanches of long-narrow systems with those of short-wide systems. If, as the above results suggested, the smallest dimension (width or length) cuts off the avalanche distribution, there should be no difference between the two cases with the same smallest dimension (360 in Fig. 8a and 720 in Fig. 8b). The data from the short-wide systems are less noisy, while the data from the long-narrow systems seem to be scattered randomly above and below the less-noisy short-wide system data. It is significant that there is no obvious, consistent (i.e., within the noise) difference between the avalanche distributions of long-narrow systems and those of the short-wide systems.

However, one should expect more avalanches in a system with a larger cut-off dimension. That is if one compared the avalanche distributions of two short-wide systems, 720 × 1440 and 360 × 2520, one should expect more avalanches in the system with the larger value of the small dimension, i.e., in the 720 × 1440 system. Fig. 9 compares the avalanche distributions of these two short-wide systems. As expected, the 720 × 1440 system has a slightly greater number of avalanches at all sizes. Not surprisingly, the number of avalanches is directly proportional to the width; however, the number of avalanches is clearly not proportional to the length.

4. Fractal dimension determinations from length-scale dependencies

In Section 2, we saw that straightforward box-counting is likely to underestimate the bulk fractal dimension of systems where the hull and bulk have different fractal

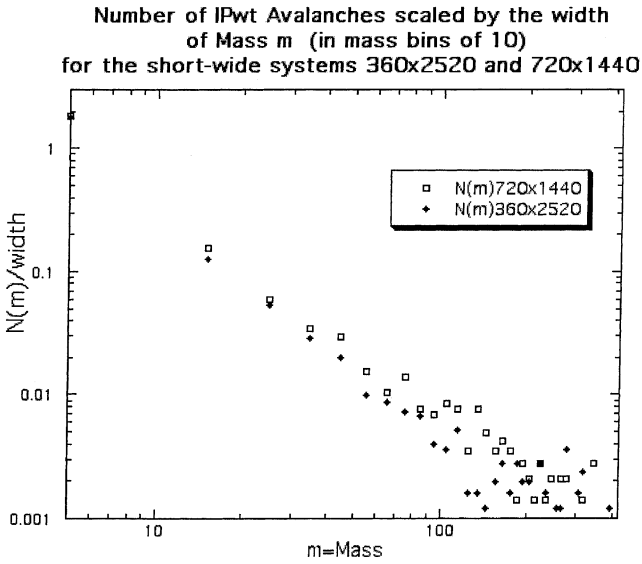

Fig. 9. The avalanches distributions of the two short-wide systems with different values of the smaller dimension, the 720 × 1440 system (□) and the 360 × 2520 system (◆) are compared. The 720 × 1440 system, with the larger value of the smaller dimension, has consistently more avalanches of all sizes up those sizes where the noise overwhelms the difference.

dimensions especially in short-wide systems where the number of hull sites represents a significant fraction of the number of bulk sites. Our ad hoc procedure for eliminating the hull–bulk competition is, at best, imperfect because it somewhat overcompensates for the competition. Although straightforward box-counting gives the best value of bulk fractal dimension for long-narrow systems, Section 3 shows that long-narrow-systems truncate the avalanche structure and, therefore, misrepresent the IP fingering. Clearly, it is advantageous to have methods for fractal dimension determination which are reliable for the short-wide systems which faithfully reproduce the IPwt fingering relevant to systems with long interfaces. In this section, we demonstrate the reliability of standard methods based directly on Eqs. (1) and (3).

The fractal dimension of a quantity can be determined from the power-law dependence of that quantity upon an appropriate length scale, i.e., as in Eq. (3). There are several quantities which could provide reasonable estimates of the length scale. In this section, we will study the dependence upon four different estimates of the length scale: (i) $\langle x_i \rangle$, the average position of the interface (external hull) in the x direction (the direction of average flow); (ii) $\langle x_m \rangle$, the average position of the mass; (iii) $W_i = \sqrt{\langle (x_i - \langle x_i \rangle)^2 \rangle}$, the average width of the interface (external hull); (iv) and the average width of the interface $W_m = \sqrt{3\langle x_m^2 \rangle - 4\langle x_m \rangle^2 + \langle x_m \rangle}$ determined from averages of the moments of the position of the injected fluid. This last expression for W_m allows the mass positions to determine the interfacial width; this was derived in an earlier

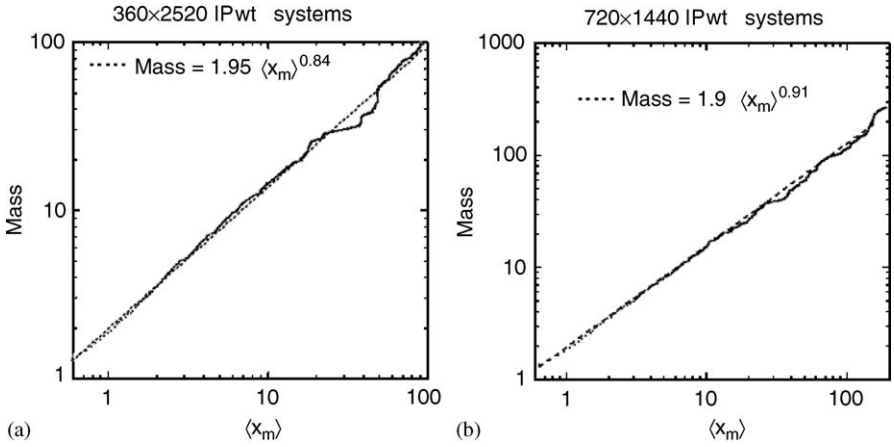

Fig. 10. The plots of mass vs. $\langle x_m \rangle$: (a) for the 360×2520 system, the best fit is $1.95\ \langle x_m \rangle^{0.84}$; (b) for the 720×1440 system, the best fit is $1.9 \langle x_m \rangle^{0.91}$. These fits indicate a value of fractal dimension in the range 1.84 to 1.91.

publication and was used to study the dependence of interfacial width upon viscosity ratio for miscible flooding where the interfaces were substantially fragmented [29].

Figs. 10a and b show fractal plots of mass vs. $\langle x_m \rangle$ for the two short-wide systems. The values determined for the fractal dimension of the bulk are consistent with the accepted values $1.80 < D_f < 1.90$. Furthermore, reasonable uncertainties in these values will span the middle of this accepted range. It should be remembered that straightforward box-counting for these short-wide systems underestimated the value of the fractal dimension, indicating values closer to $D_f \approx 1.75$.

The length of the external perimeter of a percolation cluster (number of external, unoccupied sites, which are nearest neighbors to the external hull) has a fractal dimension $D_f = \frac{4}{3}$ [24–27]. Figs. 11a and b show plots of this perimeter length vs. $\langle x_m \rangle$ for the same short-wide systems. Although the results from fits to these data are consistent with, but somewhat larger than the known value, reasonable uncertainties in these 'best-fit' values include the known value.

Similar fractal dimension determinations for the long-narrow systems provide similar results for the fractal dimensions but with greater uncertainties because these data are significantly noisier than the data from the short-wide systems, especially for the larger values of $\langle x_m \rangle$.

To show that the other lengths provide acceptable length scales for a fractal dimension determination, we need only show that they are all linearly related to $\langle x_m \rangle$. Figs. 12a and b show that the average position of the mass $\langle x_m \rangle$ and the interfacial width W_m, from mass determinations are linearly related.

The linear relationships between $\langle x_i \rangle$ and $\langle x_m \rangle$ and between W_i and W_m are both shown in Figs. 13a and b.

As expected, we have shown that the power-law dependence of a fractal quantity upon an appropriate length scale provides reliable estimates of the fractal dimension

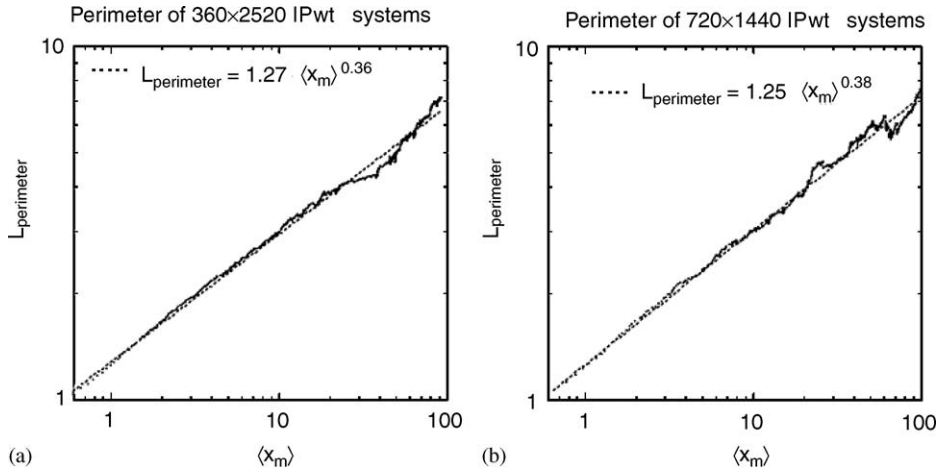

Fig. 11. The plots of external perimeter length vs. $\langle x_m \rangle$: (a) for the 360×2520 system, the best fit is $1.27\ \langle x_m \rangle^{0.36}$; (b) for the 720×1440 system, the best fit is $1.25\ \langle x_m \rangle^{0.38}$. These fits indicate a value of fractal dimension slightly larger than the exact value of $\frac{4}{3}$.

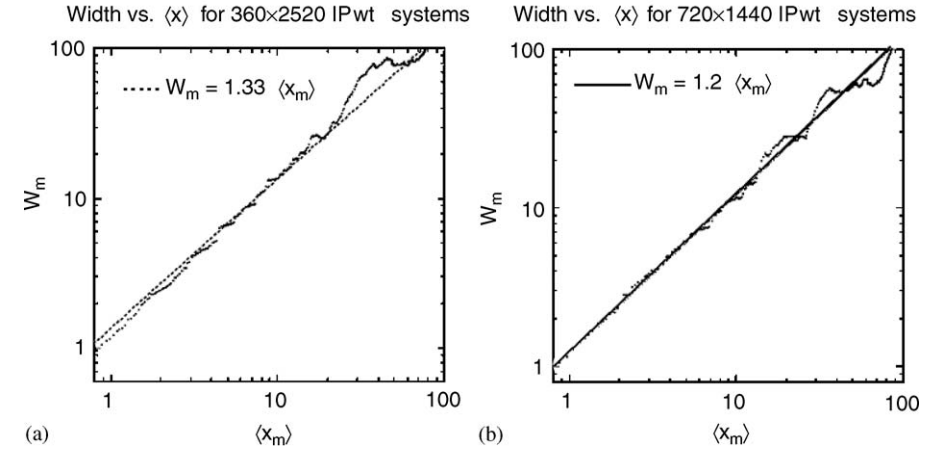

Fig. 12. The linear relation between W_m and $\langle x_m \rangle$: (a) for the 360×2520 system; the best linear fit is $W_m = 1.33 \langle x_m \rangle$; (b) for the 720×1440 system; the best linear fit is $W_m = 1.2 \langle x_m \rangle$.

for short-wide systems, without any apparent effect of the hull–bulk competition observed in box-counting for these systems. Furthermore, we showed that there are several quantities which provide reasonable estimates of the length scale: (i) $\langle x_m \rangle$, the average position of the mass; (ii) $\langle x_i \rangle$, the average position of the (external hull); (iii) $W_i = \sqrt{\langle (x_i - \langle x_i \rangle)^2 \rangle}$, the average width of the interface (external hull); and (iv) the average width of the interface $W_m = \sqrt{3\langle x_m^2 \rangle - 4\langle x_m \rangle^2 + \langle x_m \rangle}$ determined from averages of the position of the injected fluid.

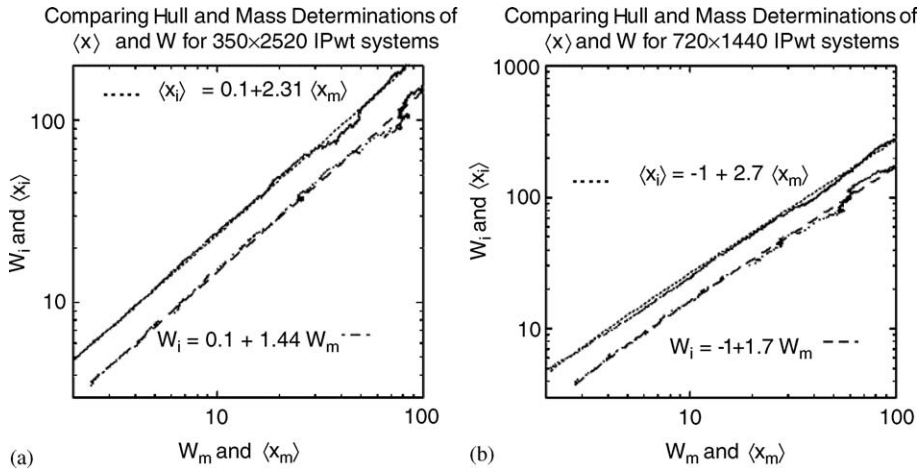

Fig. 13. The linear relationships both between $\langle x_i \rangle$ and $\langle x_m \rangle$ and between W_i and W_m: (a) for the 360×2520 system; the linear fits are given by $\langle x_i \rangle = 0.1 + 2.312\ \langle x_m \rangle$ and $W_i = 0.1 + 1.44\ W_m$; (b) for the 720×1440 system; linear fits are given by $\langle x_i \rangle = -1 + 2.70\ \langle x_m \rangle$ and $W_i = -1 + 1.70\ W_m$.

In this section, we have demonstrated that reasonable determinations of the bulk fractal dimension (or the perimeter fractal dimension) result from the use of Eq. (3) relating the mass (or perimeter length) to the length scale $\langle x_m \rangle$. Furthermore, we have shown that different length scales, $\langle x_i \rangle$, $\langle x_m \rangle$, W_i and W_m, are all linearly related as they should be for this self-similar fractal. Furthermore, we have show that these methods provide more reliable values of the fractal dimension for short-wide systems than straight-forward box-counting does.

5. Conclusions

In many of the important applications of two-phase flow in porous media, the interface can be very long so that there may be nearly as many pore bodies on the external interface as there are occupied by the injected fluid. For example, far from an injection well, where the simple IP model should be most applicable, since $N_c \approx 0$, the interface is becoming longer and longer so that there are more and more interfacial throats through which flow may occur.

In Section 2, we saw that straight-forward box-counting for the bulk significantly underestimated the value of the fractal dimension for the short-wide IPwt systems, where the number of boxes covering the outer hull, N_{hull}, is larger, i.e., comparable to the number of boxes covering the bulk. All of the results in this section support our conjectured competition between the power laws for the number of outer hull boxes and the number of bulk boxes. In an attempt to reduce this competition, we studied the power law behavior of $N_{\text{bulk}} - N_{\text{hull}}$. Although this power-law behavior slightly overestimated the values of the fractal dimension; it did allow more consistently reliable

estimates of the bulk fractal dimension from systems with widely differing aspect ratios. On the basis of all of our box-counting results, we estimate $D_f = 1.85 \pm 0.05$. Again, we emphasize that this estimate is for the relatively small systems accessible to many theoretical and experimental situations, including our own. Recent fractal dimension determinations, which (i) used systems more than 100 times larger than our million site systems and (ii) included scaling corrections to extrapolate to even larger systems, estimated the fractal dimension to be, $D_f = 1.825 \pm 0.004$ [13].

IP exhibits SOC, where one has avalanches of all sizes, at the critical point. Of course, avalanche size is truncated by the finite size of the system. In Section 3, we showed that the width of long-narrow systems truncates the avalanche structure as effectively as the length of short-wide systems; in that, systems with the same 'smaller dimension', e.g. 360×2520 and 2520×360, have the same distribution of avalanche sizes. Therefore, short-wide systems have a faithful avalanche structure over their full length; this is especially relevant to real situations with long interfaces. Although straightforward box-counting is more reliable for long-narrow systems, the avalanche structure is truncated long before the injected fluid reaches the full length of these systems. Figs. 2 and 3 show that the fingering, in the long-narrow systems with the truncated avalanche structure, is very different from the fingering in the short-wide systems with a long interface. Since short-wide systems have a more reliable avalanche structure and fingering more consistent with those real applications which have a long interface, it is important to have reliable methods of determining the fractal dimensions of these systems.

In the final section, we demonstrated that reasonable determinations of the bulk fractal dimension result from the use of Eq. (3) relating the mass to any one of several length scales. Furthermore, we have shown that this method provides more reliable values of the fractal dimension for short-wide systems than straightforward box-counting does. This method combined with the power-law behavior of $N_{bulk} - N_{hull}$ provide two reliable methods of determining the fractal dimensions of short-wide systems.

Acknowledgements

M. Ferer and Grant Bromhal gratefully acknowledge the support of the US Department of Energy, Office of Fossil Energy.

References

[1] G.L. Stegemeier, Mechanisms of entrapment and mobilization of oil in porous media, in: D.O. Shah, R.S. Schechter (Eds.), Improved Oil Recovery by Surfactant and Polymer Flooding, Academic Press, New York, 1977, p. 55.
[2] R. Chandler, et al., J. Fluid Mech. 119 (1982) 249.
[3] D. Wilkinson, J.F. Willemsen, J. Phys. A 16 (1983) 3365.
[4] D. Wilkinson, Phys. Rev. A 34 (1986) 1380–1390.
[5] D.S. Stauffer, Introduction to Percolation Theory, Taylor & Francis, Philadelphia, 1985.

[6] M. Sahimi, Flow & Transport in Porous Media & Fractured Rock From Classical Models to Modern Approaches, VCH Verlagsgesellschaft, Germany, 1994.
[7] P. Meakin, Fractals, Scaling, and Growth Far From Equilibrium, Cambridge University Press, Cambridge, 1998.
[8] M. Ferer, G.S. Bromhal, D.H. Smith, Physica A 319 (2003) 11–35.
[9] J. Feder, Fractals, Plenum Press, New York, 1988.
[10] T. Vicsek, Fractal Growth Phenomena, World Scientific, Singapore, 1989.
[11] S. Roux, E. Guyon, J. Phys. A 22 (1989) 3693–3705.
[12] L. Furuberg, et al., Phys. Rev. Lett. 61 (1988) 2117–2120.
[13] A.P. Sheppard, et al., J. Phys. A 323 (1999) L521–L529.
[14] A. Birovljev, et al., Phys. Rev. Lett. 67 (1991) 584–587.
[15] V. Frette, et al., Phys. Rev. Lett. 68 (1992) 3164–3167.
[16] M. Rosso, J.F. Gouyet, B. Sapoval, Phys. Rev. Lett. 57 (1986) 3195–3198.
[17] M.J. Blunt, Curr. Opin. Colloid Interface Sci. 6 (2001) 197–207.
[18] P. Meakin, Physica A 173 (1991) 305–324.
[19] M. Cieplak, M.O. Robbins, Phys. Rev. B 41 (1990) 11508.
[20] M.M. Dias, D. Wilkinson, J. Phys. A 19 (1986) 3131–3146.
[21] M. Ferer, G.S. Bromhal, D.H. Smith, Physica A 311 (2002) 5–22.
[22] P. Bak, C. Tang, K. Wiesenfeld, Phys. Rev. Lett. 59 (1987) 381–384.
[23] P. Bak, C. Tang, K. Wiesenfeld, Phys. Rev. A 38 (1988) 364–374.
[24] T. Grossman, A. Aharony, J. Phys. A 19 (1986) L745.
[25] P. Meakin, F. Family, 1986, unpublished.
[26] H. Saleur, B. Duplantier, Phys. Rev. Lett. 58 (1987) 2325–2328.
[27] A. Coniglio, et al., Phys. Rev. B 35 (1987) 3617.
[28] A. Bunde, J.-F. Gouyet, M. Rosso, J. Phys. A 20 (1987) 6127–6132.
[29] M. Ferer, D.H. Smith, Phys. Rev. E 49 (1994) 4114.